Heliyon 10 (2024) e25930

Contents lists available at ScienceDirect

Heliyon

journal homepage: www.cell.com/heliyon

Research article

Uranyl ammonium carbonate precipitation and conversion into triuranium octaoxide

Nguyen Trong Hung [a,**], Le Ba Thuan [a], Nguyen Thanh Thuy [a], Hoang Sy Than [b], Dinh Van Phuc [c], Jin-Young Lee [d,***], Rajesh Kumar Jyothi [e,*]

[a] Institute for Technology of Radioactive and Rare Elements (ITRRE)-VINATOM, 48 Lang Ha, Dong Da, Hanoi, Viet Nam
[b] Vietnam Atomic Energy Institute (VINATOM)-Ministry of Science and Technology (MOST), 59 Ly Thuong Kiet, Hoan Kiem, Hanoi, Viet Nam
[c] Institute of Interdisciplinary Social Sciences, Nguyen Tat Thanh University, Ho Chi Minh City, 700000, Viet Nam
[d] Resouces Utilizations Division (RUD),Korea Institute of Geoscience and Mineral Resources (KIGAM), Daejeon 34132, South Korea
[e] Hydrometallurgy Innovations Team, CSIRO Mineral Resources (CMR), 7 Conlon St. Waterford WA 6102, Perth, Australia

ARTICLE INFO

Keywords:
Uranyl ammonium carbonate (AUC)
Triuranium octaoxide (U_3O_8)
Nuclear material
Nuclear reactor
Kinetics

ABSTRACT

Uranyl ammonium carbonate (AUC), with the chemical formula $UO_2CO_3{\cdot}2(NH_4)_2CO_3$, plays a crucial role in the wet conversion of uranium hexafluoride (UF_6) into uranium dioxide (UO_2) or triuranium octaoxide (U_3O_8) for nuclear fuel production, and is used in commercial and research reactors. In this study, the precipitation of AUC from uranyl fluoride (UO_2F_2) solution and its subsequent conversion into U_3O_8 powder were investigated. AUC precipitation was performed at uranium concentrations in UO_2F_2 solution of 80–120 gL^{-1}, ammonium carbonate $(NH_4)_2CO_3$ concentrations of 200–400 gL^{-1}, and $(NH_4)_2CO_3$ to U (C/U) ratios of 5–9. The conversion of AUC into U_3O_8 powder was studied and sintering of the U_3O_8 nuclear material derived from ammonium uranyl carbonate (ex-AUC U_3O_8) was conducted at temperatures of 1000–1800 °C. The kinetics of AUC precipitation from the UO_2F_2 solution were studied using fundamental kinetic equations, and the kinetics of AUC conversion into UO_3 were examined using an isoconversion method based on the thermogravimetric analysis of AUC. The final product of U_3O_8 nuclear material was characterized using typical techniques, such as thermogravimetric analysis, X-ray diffraction, and scanning electron microscopy. This study provides valuable insights into the production and characterization of AUC and U_3O_8 nuclear materials, which are key materials in the nuclear fuel industry.

1. Introduction

Uranium dioxide (UO_2) and triuranium octaoxide (U_3O_8) are two essential nuclear fuel materials used in light-water reactors, heavy-water reactors, and research reactors. These fuel materials are important in nuclear power generation because they can produce large amounts of energy. The prospects for future nuclear power generation depend significantly on the utilization of uranium enriched at different levels. It is highly likely that this enriched uranium will serve as fuel for over 75% of the total installed capacity of nuclear

* Corresponding author.
** Corresponding author.
*** Corresponding author.
E-mail addresses: nthungvaec@gmail.com (N.T. Hung), jinlee@kigam.re.kr (J.-Y. Lee), Rajesh.Jyothi@csiro.au (R.K. Jyothi).

https://doi.org/10.1016/j.heliyon.2024.e25930
Received 9 July 2023; Received in revised form 28 January 2024; Accepted 5 February 2024
Available online 10 February 2024

power plants, based on analysis of the industry in the current century [1–5].

Nuclear research reactors encompass a wide range of civil and commercial reactors, which are predominantly employed for purposes other than power generation. This classification includes high-performance test reactors that surpass the capabilities of most other reactors. The main objective of research reactors is to serve as neutron sources for scientific investigations and other applications. These reactors are utilized for a wide range of activities, such as examining the properties and behavior of materials, analyzing neutron activation, manufacturing radioisotopes extensively used in industrial and medical fields, irradiating silicon for advanced computer applications, and numerous other research endeavors [6].

The production of nuclear fuel materials involves a range of processes to convert enriched UF_6 into powdered uranium oxides. Various methods have been developed for this purpose, including uranyl ammonium carbonate (AUC), ammonium diuranate (ADU), integrated dry route (IDR), and ammonium polyuranate (APU) processes [7–10].

Each process has advantages and disadvantages. The AUC process was developed specifically to convert UF_6 into uranium oxide powder. The AUC process has three significant benefits over the traditional ADU process. First, the uranium-oxide powders obtained from AUC precipitates have outstanding flowability, which streamlines pelletization by eliminating the need for slugging steps and the addition of lubricants. Consequently, the powder can be directly pressed into green pellets without the need for extensive intermediate procedures, such as milling, pre-compaction, granulation, or the inclusion of binders or lubricants.

Second, the uranium oxide powders from AUC precipitates are highly stable and can be sintered at high temperature, resulting in dense and durable pellets. Finally, the AUC compound is stoichiometric, whereas ADU is non-stoichiometric, and the AUC crystals tend to be larger. Consequently, soluble impurities can be efficiently eliminated through the filtration and washing of AUC particles, while this process can be problematic with ADU. Hence, the development of the AUC process has overcome some of the drawbacks of the ADU process and the challenges encountered in the production of uranium oxide powders. The AUC process is promising for the efficient and effective conversion of UF_6 into uranium oxide powder with several distinct advantages over traditional methods, such as ADU [11–16]. In contrast, the AUC process reduces the fluorine content to very low levels during the conversion of UF_6 into uranium oxides [17,18].

The wet conversion of UF_6 into uranium oxide powder by AUC precipitation involves multiple steps [19–21], beginning with the hydrolysis of UF_6, as described by the following chemical reaction (Eq. (1)):

$$UF_6\ (g) + 2H_2O\ (l) = UO_2F_2\ (aq) + 4HF\ (aq) \quad \text{(Eq. 1)}$$

The subsequent stage involves the precipitation of the AUC intermediate by introducing $(NH_4)_2CO_3$ as the precipitant, as described by Eqs. (2) and (3).

$$UO_2F_2 + 3(NH_4)_2CO_3 = UO_2CO_3{\cdot}2(NH_4)_2CO_3 + 2NH_4F \quad \text{(Eq. 2)}$$

$$2HF + (NH_4)_2CO_3 = 2NH_4F + CO_2\uparrow + H_2O \quad \text{(Eq. 3)}$$

The wet AUC cake is subsequently subjected to drying, followed by calcination in air to obtain U_3O_8 powder, which is a crucial nuclear fuel material in nuclear research reactor. The chemical reaction for the conversion of AUC into U_3O_8 powder is shown in Eq. (4).

$$3UO_2CO_3 \cdot 2(NH_4)_2CO_3 = 2UO_3.UO_2 + 4NH_3\uparrow + 5CO_2\uparrow + 2H_2O\uparrow + \frac{1}{2}\,O_2\uparrow \quad \text{(Eq. 4)}$$

Finally, U_3O_8 is reduced to produce UO_2 powder (Eq. (5)), which is a vital nuclear fuel material for both commercial and research reactors.

$$2UO_3{\cdot}UO_2 + 2H_2 = 3UO_2 + 2H_2O \quad \text{(Eq. 5)}$$

To the best of our knowledge, there is only one study on AUC precipitation from a UO_2F_2 solution [22], whereas several studies have reported the precipitation of AUC from uranyl UO_2^{2+} solutions [23–26]. Therefore, the objective of this study was to optimize AUC precipitation from the UO_2F_2+HF precursor solution to obtain a highly pure AUC precipitate of free ammonium uranyl fluoride (AUF). The objective was to identify an AUC precipitate of exceptional purity. Furthermore, previous studies have explored the conversion of AUC (and ADU) powder into ex-AUC (and ex-ADU) UO_2 powder with a range of sintering properties [27–30]. Therefore, the primary objective of this study was to provide a thorough and comprehensive study of the AUC process, specifically targeting the production of the ex-AUC U_3O_8 compound as a potential nuclear fuel material for nuclear research reactors. To accomplish this objective, we performed a systematic investigation of AUC precipitation from a UO_2F_2+HF precursor solution, as well as the subsequent conversion of the AUC precipitate into U_3O_8 powder with exceptional performance characteristics. This study provides a comprehensive analysis of the influence of various operational parameters (such as the concentration and molar ratio of the constituents) on the properties of AUC and U_3O_8 to determine the optimal conditions for AUC precipitation and U_3O_8 conversion. This knowledge is expected to contribute to improving the overall efficiency and quality of the process, leading to more precise control over the characteristics of AUC and U_3O_8 nuclear materials.

2. Materials and methods

2.1. Materials

The precipitants used in these experiments, namely, ammonium carbonate and ammonium hydroxide, were of high commercial purity (minimum of 99%) and were purchased from Shanghai Epoch Material Co., Ltd. Uranyl nitrate solution was derived from nuclear-grade pregnant stripping liquor obtained using Vietnam's yellow cake purification extraction method [27–30], which was conducted in-house by the Institute for Technology of Radioactive and Rare Elements (a part of the Vietnam Atomic Energy Institute), using tributyl phosphate as a common solvent used in the extraction of uranium. The use of nuclear-grade uranyl nitrate solution and high-purity precipitants in these experiments ensured the reliability and accuracy of the obtained results, while adhering to the safety regulations and guidelines for the handling of radioactive materials.

The UO_2F_2+HF precursor solution was prepared from a nuclear-grade uranyl nitrate solution in a series of steps. First, the uranyl nitrate solution was crystallized to obtain crystals of uranyl nitrate hexahydrate ($UO_2(NO_3)_2.6H_2O$ or UNH). The crystals were then dissolved in absolute ethanol (C_2H_5OH) and heated to 80 °C to convert the UNH into uranyl hydroxide ($UO_2(OH)_2$), as shown in Eq. (6).

$$UO_2(NO_3)_2.6H_2O + 2C_2H_5OH = UO_2(OH)_2\downarrow + 2C_2H_5ONO_2 + 6H_2O \quad \text{(Eq. 6)}$$

The yellow uranyl hydroxide compound product was filtered and washed to obtain a nitrate-free product. This product is easily dissolved in an HF solution with a U-to-HF molar ratio of 1:4 to obtain the desired UO_2F_2+HF precursor solution. The composition of this precursor solution was identical to that of the product obtained from the hydrolysis of UF_6, which also consisted of UO_2F_2 and HF in the same U-to-HF molar ratio of 1:4. The described method is considered reliable and efficient for obtaining a UO_2F_2+HF precursor solution.

2.2. AUC precipitation from UO_2F_2+HF precursor solution

Solutions of $(NH_4)_2CO_3$ with concentrations of 200, 300, or 400 gL^{-1} were used as the precipitant and 2.0 M NH_4OH solution was used to neutralize the acidic solution. Precipitation was performed in batches, in which a fixed amount of UO_2F_2+HF precursor solution with a predetermined uranium concentration (80, 100, or 120 gL^{-1}) was mixed with a specific quantity of $(NH_4)_2CO_3$ solution. The UO_2F_2+HF feed stocks were pumped into a plastic beaker, which contained a sufficient amount of 2.0 M NH_4OH solution to neutralize the HF acid present in the UO_2F_2+HF precursor solution, according to the following reaction (Eq. (7)):

$$HF + NH_4OH = NH_4F + H_2O \quad \text{(Eq. 7)}$$

Simultaneously, a given concentration of $(NH_4)_2CO_3$ precipitant was introduced into the reaction beaker using another metering pump. In most AUC precipitation experiments, the stirring speed remained constant at approximately 100 rpm, and the duration of precipitation exceeded 4 h.

Precipitation was meticulously monitored and controlled to ensure the full precipitation of soluble uranium within the reaction beaker. The resulting AUC slurry underwent a 24-h aging treatment to facilitate complete settling and enhance the purity of the AUC product. After ageing, the precipitate was filtered and washed with absolute ethanol. Subsequently, the wet AUC cake was heated in an oven at 60 °C for 5 h. This process effectively removes water and liberates ammonium carbonate, resulting in the production of a highly pure AUC product with the desired composition, which is ready for subsequent processing. To determine the AUC precipitation efficiency of each experiment, the uranium content that did not undergo precipitation was analyzed using an ICP-QQQ-MS analysis instrument (Agilent 8900). This analysis involved the application of the following mass-balance equation (Eq. 8):

$$M_p = M_i - M_f \quad \text{(Eq. 8)}$$

where M_i, M_f, and M_p (g) are the initial uranium content, amount of uranium remaining in the solution, and the amount of uranium precipitated, respectively.

And the AUC precipitation efficiency η_{AUC} was calculated using the following equation (Eq. 9):

$$\eta_{AUC} = \frac{M_i - M_f}{M_i} \times 100 \quad \text{(Eq. 9)}$$

Table 1
The experiment matrix of the study on the kinetics of AUC precipitation.

Run	No1	No2	No3
Amount of UO_2F_2 solution ([U] = 100 gL^{-1}) (ml)	120	120	120
Amount of 2 M NH_4OH solution (ml)	100	100	100
Amount of 200 gL^{-1} $(NH_4)_2CO_3$ solution (ml)	192	0	0
Amount of 300 gL^{-1} $(NH_4)_2CO_3$ solution (ml)	0	128	0
Amount of 400 gL^{-1} $(NH_4)_2CO_3$ solution (ml)	0	0	96
Total of amounts in each experiment (ml)	412	348	316

Each precipitation experiment successfully achieved satisfactory mass balance, and five replicates were performed for each experiment.

2.3. Kinetics study

The kinetics of AUC precipitation were studied at a constant temperature of 298 ± 0.2 K (controlled by a thermostat; Grant GD 100, UK), and involved simultaneously pumping 120 mL of a UO_2F_2 solution with a uranium concentration of 100 gL^{-1} and 192 mL (run No1), 128 mL (run No2), or 96 mL (run No3) of $(NH_4)_2CO_3$ solution with concentrations of 200, 300, or 400 gL^{-1}, respectively, into a 1000-mL plastic beaker containing 100 mL of a 2.0 M NH_4OH solution. The matrix experiments are listed in Table 1. During the simultaneous pumping of the UO_2F_2 and $(NH_4)_2CO_3$ solutions into a plastic beaker, the mixture was gently stirred at 100 rpm. The kinetics study commenced once both solutions were completely pumped into the beaker ($t = 0$). After specific reaction times, 0.1 mL aliquots of the mixed solution were analyzed using an ICP-QQQ-MS instrument (Agilent 8900) to determine the remaining amount of unprecipitated uranium using the mass balance equation (Eq. 8). Based on the analysis results, the amount of precipitated uranium and the kinetics of the AUC precipitation from the UO_2F_2 solution were calculated using Eq. (9). Each precipitation experiment successfully achieved satisfactory mass balance, and five replicates were performed for each experiment. The η_{AUC} at each given $(NH_4)_2CO_3$ solution concentration was employed to calculate the kinetics of AUC precipitation.

2.4. Conversion of the AUC powder into U_3O_8 powder

A Nabertherm tube furnace was used to convert AUC into U_3O_8. The furnace was operated in air for 8 h over a specific temperature range. The dried AUC powder was carefully positioned inside the furnace to initiate conversion. Rigorous monitoring was conducted to ensure that the optimal conditions were maintained.

2.5. Characterization of the AUC and U_3O_8 powders

X-ray diffraction (XRD) analysis was conducted using a Siemens D5005 instrument with monochromatized Cu Kα radiation (λ = 0.15418 nm) to assess the quality and crystal phases of the samples. This method provides valuable information on the crystal structure and purity of samples. To gain insights into the composition, purity, and thermal stability of the AUC samples, thermogravimetric analysis (TGA) and differential thermal analysis (DTA) were performed using a SETARAM thermal analyzer. Scanning electron microscopy (SEM; JEOL-IT100LV, Horiba, Japan) was used to visualize the morphology of the AUC and U_3O_8 powders. Additionally, laser scattering methods using a PARTICA LA-960 instrument (Horiba, Japan) were employed to determine the particle size distributions of the powders. By combining these analytical approaches, a comprehensive understanding of the characteristics of the AUC and U_3O_8 powders was achieved, enabling optimization of the process and material characteristics.

3. Results and discussion

3.1. AUC precipitation process

In previous research, Kan-Sen Chou et al. [22] studied AUC precipitation, specifically the effects of the reaction and aging temperatures on the process. The results of their investigation highlighted the significant role of these temperatures in determining the AUC precipitation efficiency during batch precipitation. The AUC precipitation efficiency was significantly influenced by the reaction and aging temperatures within the analyzed range. The results indicated that the maximum precipitation efficiency achieved for uranium was below 80%, implying a relatively high solubility of AUC in the ammonium carbonate solution. These findings shed light on the behavior of AUC during precipitation and provide important insights for further process optimization. The observed decrease in uranium precipitation efficiency as the reaction and aging temperatures increases aligns is consistent with the observation that the precipitation efficiency primarily depends on the solubility of AUC in the final solutions. Although the AUC precipitation efficiency showed minimal variation with aging time, it is important to note that other characteristics of the precipitate, including the composition, surface properties, and particle size distribution, change during aging. Therefore, in our study on the precipitation of AUC from a UO_2F_2 solution, we specifically excluded the influence of temperature and aging time on AUC precipitation. Instead, we focused on investigating the effects of key technological parameters, namely the uranium concentration in the initial UO_2F_2 solution, the concentration of the precipitating agent $(NH_4)_2CO_3$, and the molar ratio of $(NH_4)_2CO_3$/U (C/U), as these factors have a substantial influence on AUC precipitation.

3.1.1. Effect of uranium concentration in the stock UO_2F_2 solution and concentration of the precipitating agent $(NH_4)_2CO_3$ on AUC precipitation

Kim et al. [31] specifically investigated the influence of the uranium concentration in a stock $UO_2(NO_3)_2$ solution and the concentration of the precipitating agent $(NH_4)_2CO_3$ on the morphology and chemical composition of AUC precipitates. They observed that the morphologies of the AUC precipitates were dependent on the processing conditions. When the uranium concentration exceeded 80 gL^{-1} and the ammonium carbonate concentration was above 200 gL^{-1}, with a molar ratio of $(NH_4)_2CO_3$/U (C/U) greater than 5 and a pH above 7.6, the AUC precipitates exhibited a distinct monoclinic morphology. In the range of 80–120 gL^{-1} ammonium carbonate, a C/U of 4–5, and a pH of 7.3–7.5, the AUC precipitates displayed a needle-like morphology. In contrast, for concentrations of ammonium

carbonate from 60 to 80 gL^{-1}, a C/U of 3.5–4.0, and a pH of 7.0–7.3, the AUC precipitates showed a flake-like morphology. These findings highlight the significant influence of uranium and ammonium carbonate concentrations on the morphology of AUC precipitates. Finally, for an ammonium carbonate concentration of 40–60 gL^{-1}, a C/U below 3.5, and pH below 4.0, the AUC precipitate particles were irregular. XRD, infrared (IR) spectroscopy, and thermal analyses were employed to gain a deeper understanding of the chemical composition and structure of these precipitates. The results confirmed that the characteristic monoclinic crystal structures of the AUC precipitates were $(NH_4)_4UO_2(CO_3)_3$. The orthorhombic crystal structure corresponds to that of ammonium uranate. In contrast, the AUC precipitates with needle- and flake-like morphologies were mostly amorphous and lacked a well-defined crystalline arrangement. Nonetheless, the AUC precipitates demonstrated a high degree of crystallinity overall, which facilitated filtration or removal of soluble impurities during subsequent processing steps.

In a study conducted by Boualia et al. [32], the effect of excess ammonium carbonate on the uranium concentration in the AUC leaching solution was examined. They discovered that, as the amount of excess $(NH_4)_2CO_3$ in the solution increased, the uranium concentration in the mother solution decreased. This decrease ultimately led to the complete crystallization of the AUC precipitate. Additionally, researchers have noted a significant reduction in the solubility of the AUC within the $(NH_4)_2CO_3$ concentration range of 200–400 gL^{-1}. These findings suggest that the presence of excess ammonium carbonate plays a crucial role in promoting the precipitation and crystallization of AUC while simultaneously reducing its solubility in the solution.

Based on the findings of the literature review, the experimental conditions for AUC precipitation were determined. The uranium concentration in the stock UO_2F_2 solution was set within the range of 80–120 gL^{-1}, while the analyzed concentration of the $(NH_4)_2CO_3$ precipitating agent was 200–400 gL^{-1}. These ranges were chosen based on previous studies that demonstrated favorable AUC precipitation under these conditions. Furthermore, to maintain consistency and ensure optimal results, the C/U molar ratio was fixed at 8 throughout the experiments. By controlling these parameters, it was anticipated that AUC precipitation would yield satisfactory results and facilitate the subsequent conversion of AUC into U_3O_8 powder.

To effectively optimize the impact of the uranium concentration in the UO_2F_2 solution and the $(NH_4)_2CO_3$ concentration on AUC precipitation, a response surface methodology (RSM) utilizing a central composite face-centered (CCF) design was employed. In this methodology, influential variables were selected; X_1 represents the uranium concentration in the UO_2F_2 solution and X_2 represents the $(NH_4)_2CO_3$ concentration (gL^{-1}). The AUC precipitation efficiency (Y, %) was used as the dependent variable. A quadratic function was used to establish the relationship between the variables, as described in Eq. (10), and determine the precise impact of independent variables on AUC precipitation to aid the optimization of the desired outcome.

$$Y = b_0 + b_1X_1 + b_2X_2 + b_{11}X_1^2 + b_{22}X_2^2 + b_{12}X_1X_2 \quad \text{(Eq. 10)}$$

In this equation, the constant coefficient (b_0), linear coefficient (b_i), quadratic coefficient (b_{ii}), and interaction coefficient (b_{ij}) hold their respective roles and values. The influential variables X_1 and X_2 in the equation were set to values of 1, 0, and −1 to represent high, central, and low experimental conditions, respectively. The set values were correlated with the actual experimental values. Table 2 provides an overview of the corresponding set values and the corresponding experimental values for X_1 and X_2 to enable easy reference during the analysis and interpretation of the experimental results. To determine the optimal combination of these factors for achieving the highest AUC precipitation efficiency, nine experimental runs were required. The calculation formula was derived as $2^k + 2k + n_0$, where k is the number of factors (two in this case) and n_0 is the number of replications at the center points, which was set to one for this particular study. Table 2 lists the experimental matrices within the experimental range used in this study. Nine runs were necessary to obtain sufficient data for the analysis and to identify the most effective combination of the uranium concentration in the UO_2F_2 solution and $(NH_4)_2CO_3$ concentration to achieve the highest possible AUC precipitation efficiency. By carefully controlling these variables, it is possible to optimize AUC precipitation and maximize the production of high-quality products.

Table 2 displays the outcomes of the 9 experimental trials, highlighting the results obtained from various tests. To analyze and construct a model, the obtained results were input into MODDE software (version 5.0) and multiple linear regressions were applied. To assess the suitability of the quadratic model, a significance test and analysis of variance (ANOVA) were conducted. Table 3 provides a detailed overview of the estimated regression coefficients and their corresponding 95% confidence intervals. This comprehensive summary provides valuable information about the adequacy of the model and its predictive capabilities.

Table 2
Central composite rotatable design arrangement and results.

Run	Coded levels				Responses	
	Coded levels		Real values (gL^{-1})		Experimental (Actual), in %	Calculated (Predicted), in %
	X_1	X_2	U concentration	$(NH_4)_2CO_3$ concentration		
1	−1	−1	80	200	88.6 ± 0.5	87.9
2	1	−1	120	200	94.7 ± 0.3	94.3
3	−1	1	80	400	93.3 ± 0.6	93.2
4	1	1	120	400	96.6 ± 0.2	96.7
5	−1	0	80	300	89.9 ± 0.8	90.7
6	1	0	120	300	95.4 ± 0.4	95.6
7	0	−1	100	200	90.7 ± 0.7	91.7
8	0	1	100	400	95.6 ± 0.3	95.6
9	0	0	100	300	94.8 ± 0.5	93.8

Table 3
Estimated regression coefficients for sequential model.

Source	Coefficient	Standard error	p-value
Model	93.7778	0.495564	1.34612×10^{-6}
X_1	2.48333	0.435748	0.0107131
X_2	1.91666	0.435749	0.0217824
X_1^2	−0.616663	0.754739	0.473747
X_2^2	−0.116674	0.754739	0.88696
X_1X_2	−0.699996	0.533681	0.280989

As shown in Table 3, the coefficients b_{11} (representing X_1^2), b_{22} (representing X_2^2), and b_{12} (representing X_1X_2) have p-values exceeding 0.05, indicating a lack of statistical significance. Consequently, these coefficients were deemed insignificant and were rejected from the model. This implies that the effects of the quadratic coefficients b_{11}, b_{22}, and b_{12} on the response variable Y are not meaningful or influential. To assess the precision and variability of the model, the coefficient of determination (R^2) was calculated, resulting in a value of 0.95, indicating a high level of consistency. Moreover, the ANOVA results provide the p-value, sum of squares, mean square, model significance (F-value), and degrees of freedom. The p-value for the regression model was 0.05, indicating the significance of the model terms at the 95% confidence level. Consequently, the established model is considered statistically robust and reliable. The lack-of-fit p-value, assessed at the 0.05% level, did not show statistical significance, suggesting that the model did not suffer from a significant lack-of-fit. This further supports the validity and adequacy of the proposed model. The final equation for AUC precipitation, incorporating the set coefficients (Eq. (10)) is represented as follows (Eq. (11)):

$$Y(\%) = 93.8 + 2.5X_1 + 1.9X_2 \quad \text{(Eq. 11)}$$

The AUC precipitation efficiency values displayed in Table 2 were determined using Eq. (11). The results show an excellent correspondence between the calculated values and experimentally determined values, indicating that the RSM-CCF model for AUC precipitation describes the observed experimental data well, thereby providing additional support for reliability and consistency of the data. Eq. (11) shows the effect of the linear coefficient b_1 (associated with X_1) on the response variable Y, which was $b_0 + 2.5\%$ for a uranium concentration of 100–120 gL^{-1}. Similarly, the contribution of the linear coefficient b_2 (associated with X_2) on Y was $b_0 + 1.9\%$ for the $(NH_4)_2CO_3$ concentration range of 300–400 gL^{-1}. These observations provide valuable insights into the relationship between the input variables and the output response in AUC precipitation. The relationship between the uranium concentration, $(NH_4)_2CO_3$ concentration, and AUC precipitation efficiency is linear, indicating that increases in both the uranium and $(NH_4)_2CO_3$ concentrations results in a higher precipitation efficiency. This correlation is visually represented in Fig. 1, which presents a contour plot showing the AUC precipitation efficiency as a function of the uranium and $(NH_4)_2CO_3$ concentrations. The maximum AUC precipitation efficiency achieved through AUC precipitation reaches approximately 98%. This optimal precipitation efficiency is attained when the uranium concentration in the UO_2F_2 solution and the $(NH_4)_2CO_3$ concentration are 120 and 400 gL^{-1}, respectively. These findings highlight the significance of uranium and $(NH_4)_2CO_3$ concentrations in determining the efficiency of AUC precipitation, with higher concentrations resulting in enhanced uranium precipitation efficiency.

Fig. 2 shows the particle size distribution of AUC powder obtained with the various UO_2F_2 solutions. The AUC precipitation experiments were conducted with a fixed $(NH_4)_2CO_3$ precipitant concentration of 400 gL^{-1}. Within the uranium concentration range of 80–100 gL^{-1}, the average particle size of the AUC powder is approximately 24 μm; however, as the uranium concentration increases to 120 gL^{-1}, the average particle size of the AUC powder significantly decreases to approximately 14 μm (Fig. 2). This suggests that higher

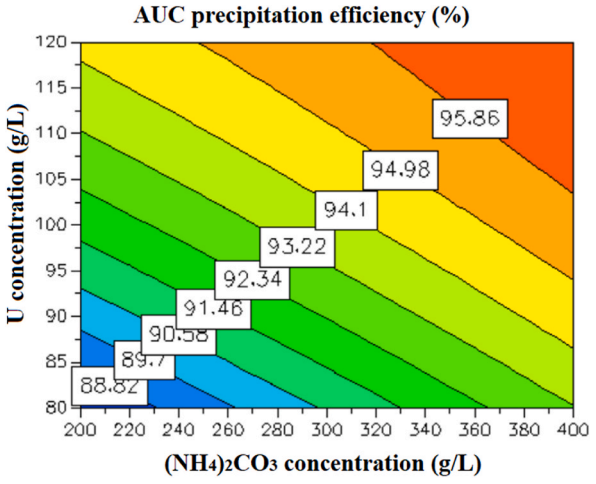

Fig. 1. Contour plot of AUC precipitation efficiency vs U and $(NH_4)_2CO_3$ concentrations.

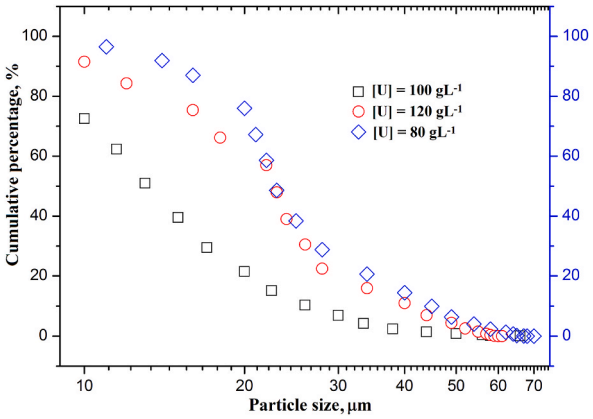

Fig. 2. Influence of uranium concentration on the AUC particle size.

uranium concentrations during AUC precipitation tend to result in smaller AUC particles, which is explained as follows. Considering both kinetic and thermodynamic factors, lower concentrations of interacting ions, combined with a higher ionic strength of spectator salts, results in reduced activity coefficients, which result in lower precipitation rates and hence, larger crystals. These findings are in good agreement with those of a previous study [33], providing additional support for the observed influence of the precursor concentration on particle size. This information provides valuable insight into the relationship between the uranium concentration and the resulting particle size of the AUC powder.

Previous studies [13,22] showed that an increase in the particle size of the AUC powder enhances the efficiency of impurity removal from uranium during the subsequent stages of AUC precipitate filtration and washing. In this study, the impurities in the AUC precipitate samples prepared using various uranium concentrations in the UO_2F_2 solution were analyzed. As shown in Table 4, the impurity contents in the AUC precipitate samples obtained using uranium concentrations of 80–100 gL^{-1} are lower than that observed in the AUC precipitate sample obtained at a uranium concentration of 120 gL^{-1}. Comparing the data presented in Table 4 with the specifications outlined in ASTM C776-06: Standard Specification for Sintered Uranium Dioxide Pellets, shows that the AUC precipitate samples with lower impurity contents exceed the standard requirements. Therefore, the AUC precipitates prepared here are suitable for the fabrication of ceramic uranium oxides used in nuclear fuel production. Based on the findings of this study, the optimal conditions for AUC precipitation (~96% precipitation efficiency) are a uranium concentration of 100 gL^{-1} in the UO_2F_2 solution and a $(NH_4)_2CO_3$ concentration of 400 gL^{-1}.

3.1.2. *Effect of the molar ratio of C/U on AUC precipitation*

To investigate the effect of the C/U molar ratio on AUC precipitation, C/U ratios from 5 to 9 were examined to gain valuable insights into the processing conditions required to achieve the desired AUC precipitate characteristics. Precipitation experiments were conducted with a fixed uranium concentration of 100 gL^{-1} in the UO_2F_2 solution and a $(NH_4)_2CO_3$ precipitant concentration of 400 gL^{-1}. Fig. 3 shows the XRD spectrum of the AUC precipitated at a C/U of 5, from which the intermediate product was preliminarily identified as $(NH_4)_2UF_8$ (AUF). The AUF crystals exhibit an orthorhombic structure that aligns closely with the reference AUF pattern provided by ASTM (No. 21–802) [22], with lattice constants of $a = 6.305$ Å, $b = 13.431$ Å, and $c = 9.018$ Å, and angles of $\alpha = \beta = \gamma = 90°$. In contrast, the AUC crystals had a monoclinic structure, characterized by an XRD peak at $2\theta = 14°$ and space group $C2/c$, in accordance with the results of previous studies. The lattice constants of the AUC crystals were $a = 10.68$ Å, $b = 9.38$ Å, and $c = 12.85$ Å, with angles of $\alpha = \gamma = 90°$ and $\beta = 96.45°$, which are very similar to those reported in previous studies [34–36]. Chou et al. [22]

Table 4
Impurities composition in AUC precipitate samples.

Impurities	Impurities composition, in ppm				Analysis method
	Sample 1*	Sample 2*	Sample 3*	ASTM C776-06	
Aluminum	126	138	186	250	ICP-MS
Calcium + magnesium	72	61	95	200	
Chromium	below detection	below detection	12	250	
Cobalt			8	100	
Iron	58	66	72	500	
Nickel	0.8	1	3	250	
Silicon	114	98	164	500	
Rare earths, Thorium, Boron, Cadmium	below detection			<10	

*Sample 1 is AUC precipitated at U concentration of 80 gL^{-1}.
*Sample 2 is AUC precipitated at U concentration of 100 gL^{-1}.
*Sample 3 is AUC precipitated at U concentration of 120 gL^{-1}.

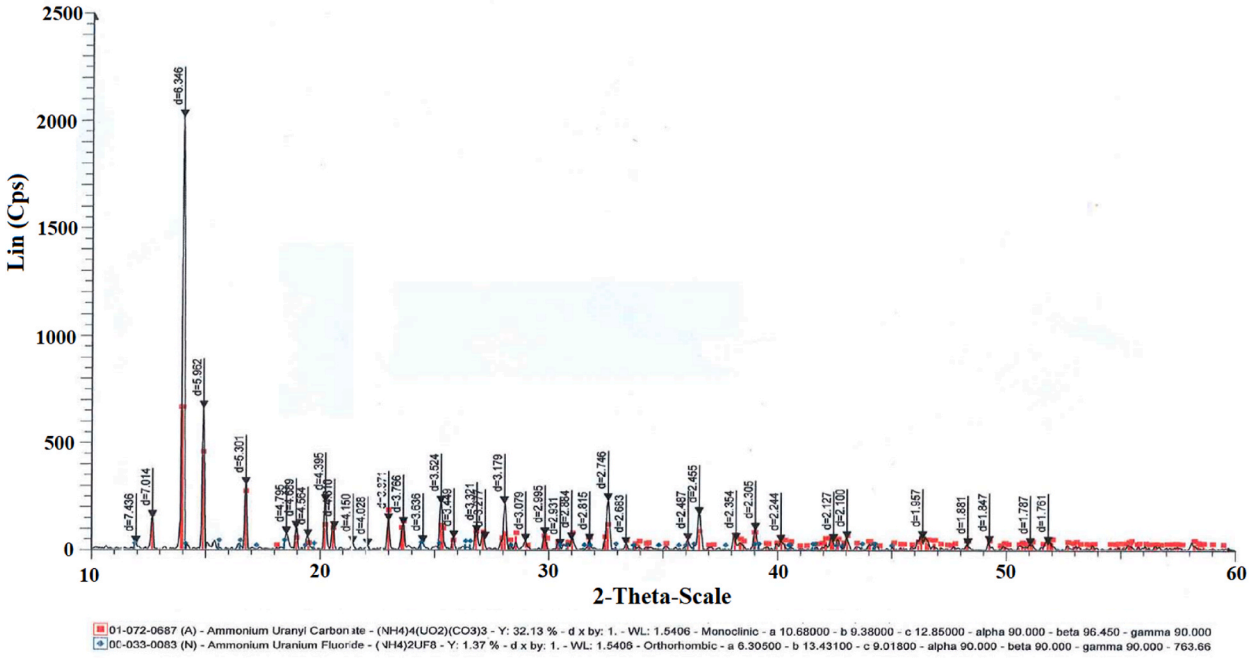

Fig. 3. The XRD spectrum of the AUC precipitated at the C/U molar ratio of 5.

similarly confirmed the orthorhombic and monoclinic structures of the AUF and AUC precipitates, respectively. Unlike the ADU intermediate in the UNH–$(NH_4)_2CO_3$ system, which dissolves prior to the formation of AUC particles, the AUF intermediate in this particular case can coexist with the AUC for a certain amount of time. This implies that the dissolution of AUF is a comparatively slow process. Further detailed investigations are required to gain a more comprehensive understanding of the formation and dissolution mechanisms of AUF in ammonium carbonate solutions.

Fig. 4 shows an XRD pattern of AUC powder precipitated at a C/U of 7. The XRD pattern shows a peak at $2\theta = 14°$ corresponding to AUC with a monoclinic structure (space group $C2/c$) and lattice constants of $a = b = 10.06$ (1) Å and $c = 12.86$ (2) Å, and angles of $\alpha = \gamma = 90°$ and $\beta = 96.42°$. These results are consistent with those previously reported [34–36], corroborating the accuracy and consistency of the observed AUC crystal structures. Fig. 4 shows an SEM micrograph of a typical AUC crystal.

The AUC powder was subjected to TGA, as shown in Fig. 8. The mass-loss curve reveals that the decomposition of AUC occurs at a temperature of 217 °C, corresponding to a mass loss of approximately 44%. By analyzing this mass variation, the material balance calculations unequivocally indicated that the AUC compound was $(NH_4)_4UO_2(CO_3)_3$. Consequently, our study successfully identified the conditions conducive to the formation of AUC precipitates, which are very similar to the findings reported in the literature [37–42]. Therefore, to achieve the precipitation of free AUF, a C/U molar ratio greater than six is required. However, the uranium precipitation

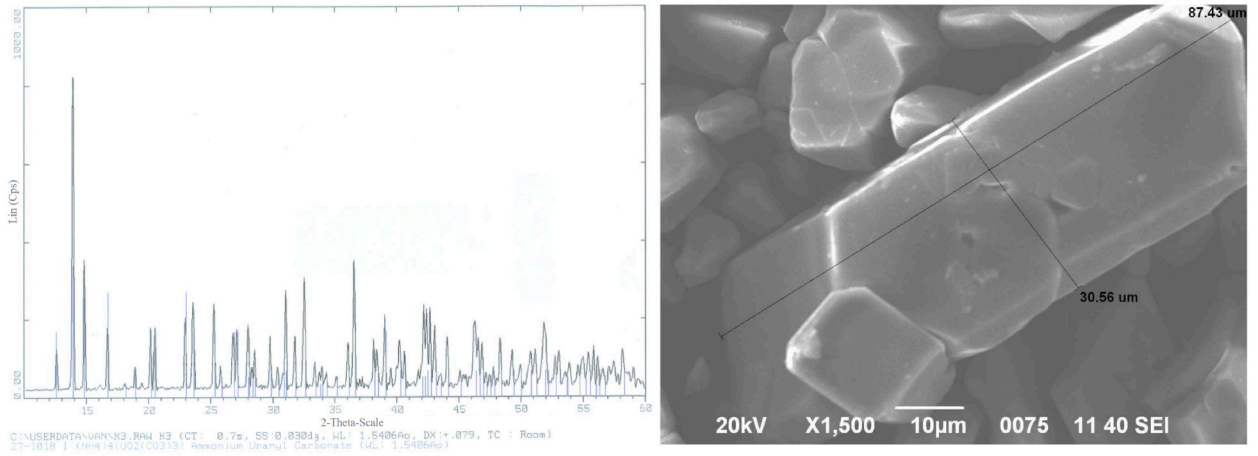

Fig. 4. The XRD spectrum of the AUC precipitated at the C/U molar ratio of 7 (left) and the SEM microphotograph of a AUC crystal (right).

efficiency at C/U values of 6–7 was approximately 95%, which is lower than that at C/U values of 8–9, which exceeded 96%. Interestingly, the particle sizes of the AUC precipitates prepared using the two ratios were similar. Fig. 5 illustrates the particle size distribution of the AUC powder at the C/U molar ratios of 6 and 9, with an average particle size of approximately 24 μm. To optimize the chemical usage and minimize the waste treatment requirements, a C/U of 8 was chosen for optimal AUC precipitation.

3.2. Kinetics of AUC precipitation from UO_2F_2+HF solution

Because the AUC precipitate is dissolved in the $(NH_4)_2CO_3$ solution, the AUC precipitation reaction using an $(NH_4)_2CO_3$ solution as the precipitant is a reversible reaction, where the reaction shown in Eq. (2) can be rewritten as follows (Eq. (12)):

$$UO_2F_2 + 3(NH_4)_2CO_3 \underset{reverse}{\overset{forward}{\rightleftharpoons}} UO_2CO_3{\cdot}2(NH_4)_2CO_3 + 2NH_4F \quad \text{(Eq. 12)}$$

The AUC precipitation reaction occurs when the rate of AUC precipitation (forward reaction) is greater than that of AUC dissolution (reverse reaction). The reaction shown in Eq. (12) ends when the forward and reverse reaction rates become equal and the reaction system reaches equilibrium. In Section 3.1, the study of AUC precipitation parameters showed that the AUC precipitate of free AUF is only formed at C/U > 6, which is twice the stoichiometric ratio of Eq. (12). However, the efficiency of AUC precipitation depends on the concentration of the $(NH_4)_2CO_3$ precipitate; as the concentration of the precipitate increases, the solubility of the AUC precipitate decreases, resulting in a higher precipitation efficiency.

The kinetics studies on AUC precipitation were conducted over a range of $(NH_4)_2CO_3$ precipitant concentrations (200–400 gL^{-1}) at a standard temperature of 298 K (25 °C), with the uranium concentration in the UO_2F_2 solution and the C/U ratio fixed at 100 gL^{-1} and 8, respectively. Fig. 6 illustrates the efficiency of AUC precipitation depending on the precipitation time. At a precipitant concentration of 200 gL^{-1}, the AUC precipitation efficiency reached approximately 92% after 150 min of reaction, after which the precipitation efficiency increased very slowly. Meanwhile, at precipitant concentrations of 300–400 gL^{-1}, the AUC precipitation efficiency reached 93–95% at the same precipitation time and remained nearly unchanged thereafter, implying that the system had reached equilibrium. Thus, at low precipitant concentrations, the AUC precipitate dissolved well in the carbonate solution, resulting in lower precipitation efficiency and longer precipitation times.

Based on these results, kinetic calculations for the precipitation process were conducted using the following equations (Eqs. (13)–(15)) to determine the reaction rates [43]:

First order:

$$\frac{dC_t}{dt} = k_1(C_0 - C_t) \quad \text{(Eq. 13)}$$

Second order:

$$\frac{dC_t}{dt} = k_2(C_0 - C_t)^2 \quad \text{(Eq. 14)}$$

Third order:

$$\frac{dC_t}{dt} = k_3(C_0 - C_t)^3 \quad \text{(Eq. 15)}$$

Here, the reaction rate constant is denoted as k_n ($L^{(n-1)}mol^{(1-n)}min^{-1}$), where n is the reaction order, C_0 is the initial concentration of uranium ($molL^{-1}$), and C_t is the amount of precipitated uranium ($molL^{-1}$).

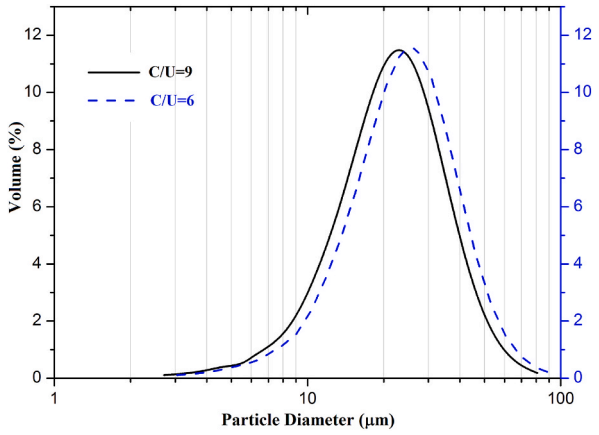

Fig. 5. The particle size distribution of the AUC crystal precipitated at the C/U molar ratios of 6 and 9.

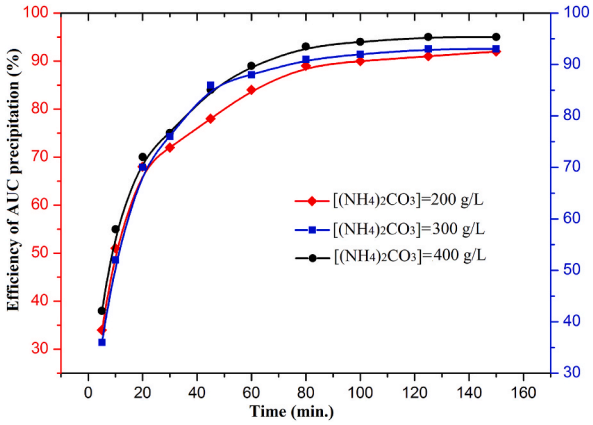

Fig. 6. The efficiency of AUC precipitation vs the precipitation time during precipitation AUC at T = 298K, [U] in UO_2F_2 solution = 100 gL^{-1} and C/U molar ratio = 8).

Upon integration, the subsequent expressions are obtained:
First order (Eq. 16):

$$k_1 = \frac{1}{t} ln \frac{C_0}{C_0 - C_t} \quad \text{(Eq. 16)}$$

Second order (Eq. (17)):

$$k_2 = \frac{1}{t} \frac{C_t}{C_0(C_0 - C_t)} \quad \text{(Eq. 17)}$$

Third order (Eq. (18)):

$$k_3 = \frac{1}{2t} \left\{ \left(\frac{1}{(C_0 - C_t)^2} \right) - \left(\frac{1}{C_0^2} \right) \right\} \quad \text{(Eq. 18)}$$

Table 5 shows the reaction rate constants obtained for different precipitant concentrations. The second-order reaction rate constant k_2 was similar for all concentrations, whereas k_1 and k_3 varied. This suggests that the AUC precipitation reaction under investigation followed second-order kinetics. To determine the precise value of k_2, the slope of a plot of $\frac{1}{(C_0 - C_t)}$ versus time (Fig. 7) was calculated using linear regression analysis, resulting in an average k_2 of 0.258 $Lmol^{-1}min^{-1}$.

In a previous study on the precipitation of AUC from a uranyl nitrate solution [43], it was determined that AUC precipitation followed second-order kinetics, with k_2 values of 0.310 and 0.437 $Lmol^{-1}min^{-1}$ at temperatures of 313.15 and 330.15 K, respectively. Thus, the k_2 values of the AUC precipitation reaction from the UO_2F_2 solution are lower than those from the uranyl nitrate solution. This is attributed to the large excess of $(NH_4)_2CO_3$ precipitant required for AUC precipitation from the UO_2F_2 solution, causing the AUC precipitate to dissolve in the carbonate solution, which reduces k_2. These kinetic results for AUC precipitation are expected to be useful in the optimization of the reaction conditions, design of efficient processes, improvement of product quality, and provide fundamental insights into the reaction mechanisms involved.

3.3. Conversion of AUC into U_3O_8

3.3.1. Conversion of AUC into UO_3

The TG–dTG curves of the AUC powder obtained at heating rate of 10 °$Cmin^{-1}$ in air are presented in Fig. 8. The typical dTG and TG curves of the AUC decomposition reaction obtained under these conditions are similar to those described in the literature [37–42]. The dTG and TG curves obtained during AUC decomposition (Fig. 8) are similar to those reported in the literature, indicating typical behavior. The decomposition reaction involves the formation of intermediate compounds, specifically, UO_3. When AUC is treated in air, the final product is U_3O_8, as reported previously [37–42].

By analyzing the TG and dTG curves, we observed the weight loss and peak maximum temperature during the decomposition of AUC in air. AUC decomposition begins around 150 °C and continues until 350 °C. The formation of anhydrous UO_3 occurs when the temperature reaches approximately 400 °C, coinciding with an exothermic peak on the dTG curve at a temperature of 217.2 °C. Fig. 8 also depicts the percentage mass loss (TG) and the mass loss rate (dTG) curves as a function of temperature for the thermal decomposition of AUC under an air environment, with a heating rate of 10 °$Cmin^{-1}$. These curves show that the thermal decomposition of AUC in air at this heating rate occurs in a single step. The decomposition reaction of AUC in air is summarized as follows (Eq. (19)) [37–42]:

Table 5
The AUC precipitation rate constants.

Time (min)	$[(NH_4)_2CO_3]$								
	200 gL^{-1} (No1)			300 gL^{-1} (No2)			400 gL^{-1} (No3)		
	k_1 (min^{-1})	k_2 ($Lmol^{-1}min^{-1}$)	k_3 ($L^2mol^{-2}min^{-1}$)	k_1 (min^{-1})	k_2 ($Lmol^{-1}min^{-1}$)	k_3 ($L^2mol^{-2}min^{-1}$)	k_1 (min^{-1})	k_2 ($Lmol^{-1}min^{-1}$)	k_3 ($L^2mol^{-2}min^{-1}$)
5	0.083	0.245	0.734	0.090	0.268	0.816	0.096	0.292	0.907
10	0.071	0.248	0.896	0.073	0.258	0.946	0.080	0.291	1.115
20	0.057	0.253	1.241	0.060	0.278	1.432	0.060	0.278	1.432
30	0.042	0.204	1.110	0.048	0.251	1.545	0.046	0.238	1.416
45	0.034	0.188	1.237	0.044	0.325	3.148	0.041	0.278	2.400
60	0.031	0.208	1.800	0.034	0.265	2.746	0.037	0.321	3.854
80	0.028	0.241	2.890	0.030	0.301	4.335	0.033	0.395	7.190
100	0.023	0.214	2.804	0.025	0.274	4.397	0.028	0.373	7.839
125	0.019	0.193	2.775	0.021	0.253	4.601	0.024	0.362	9.040
150	0.017	0.182	2.931	0.018	0.211	3.834	0.020	0.301	7.534

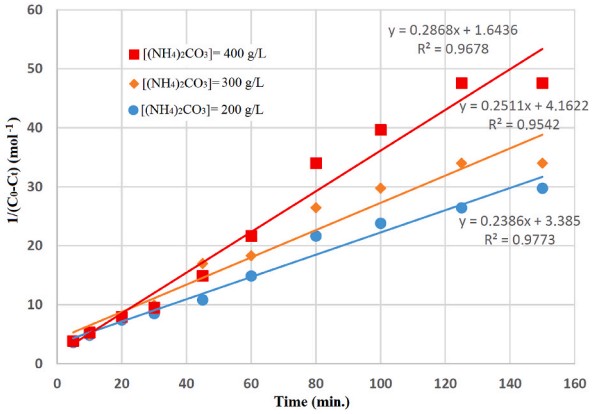

Fig. 7. Graphical determination of the mean rate constants value.

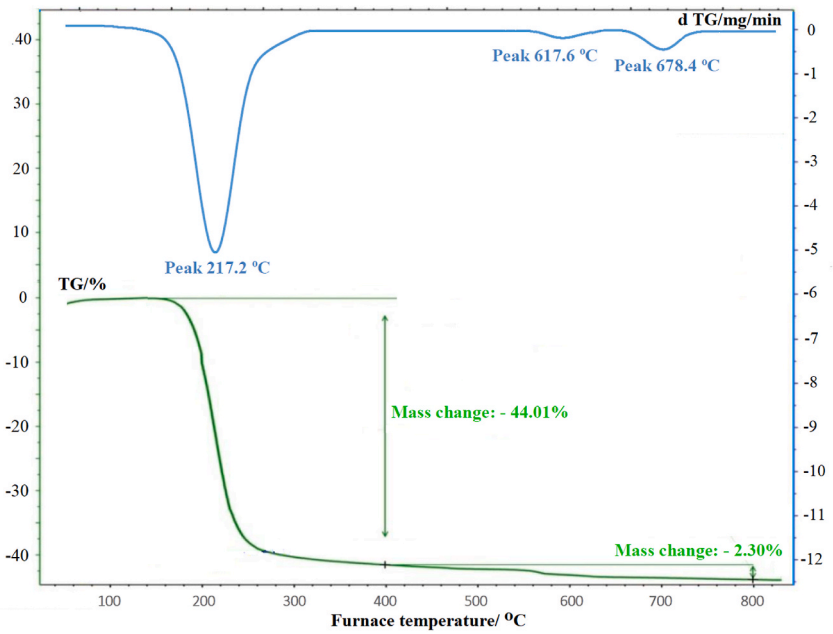

Fig. 8. The TG-dTG curve of the AUC.

$$(NH_4)_4UO_2(CO_3)_3 = UO_3 + 4NH_3 + 3CO_2 + 2H_2O \quad \text{(Eq. 19)}$$

The calculated weight loss in air was 44.01%.

Numerous previous studies [37–42] explored the decomposition of AUC in different environments, such as O_2, Ar, N_2, and 90% Ar–10% H_2 mixtures. Our TG–dTG curves obtained at a heating rate of 10 °Cmin^{-1} in oxygen and inert gases (argon and nitrogen) were similar to those reported in the literature. Within the temperature range of 100–900 °C, the shapes of the TG–dTG curves were similar for the various gases, with the exception of the 90% Ar–10% H_2 mixture. Irrespective of the environment, the same reaction occurred, leading to the formation of UO_3 as the intermediate compound. The final product of treating AUC with either oxygen or an inert gas was U_3O_8. Additionally, the literature results indicate that AUC begins to decompose at approximately 135 °C in all environments, whereas our study suggests a value of approximately 150 °C.

According to previous studies [37–42], AUC decomposition can lead to the formation of several intermediate compounds before the crystallization of UO_3, including $(UO_3(H_2O)_{1.5}$, $UO_3(H_2O)$, $UO_3(H_2O)_{0.65}$, $UO_3(H_2O)_{0.5}$, and $UO_3(H_2O)_{0.25}$. These studies also indicate that the thermal decomposition of AUC in an O_2 environment and a heating rate of 10 °Cmin^{-1} occurs in a single step at approximately 200 °C; however, our findings suggest that decomposition occurs at 217 °C, which is consistent with Eq. (19).

The mass losses related to AUC decomposition before UO_3 crystallization in Ar, N_2, O_2, and 90% Ar–10% H_2 were 44.20%, 44.35%, 44.05%, and 44.95%, respectively. Thus, mass loss of 44.01% in air (in our study) is very similar to that of 44.05% obtained in O_2 (in the previous studies [37–42]).

3.3.2. Kinetics of AUC decomposition into UO_3

The activation energies of the thermal decomposition of AUC are often calculated using the isoconversion method [40–44]. This method involves analyzing the reciprocal temperature at which a specific fraction of conversion is attained in experiments conducted at different constant heating rates. The rate of thermal decomposition is influenced by factors such as the conversion fraction ($\alpha = 0$–1), temperature (T), and time (t). In condensed-phase processes, the most widely used model for rate estimation is as follows (Eq. (20)):

$$\frac{d\alpha}{dt} = f_{(\alpha)} k_{(T)} \quad \text{(Eq. 20)}$$

Here, $\frac{d\alpha}{dt}$ is the rate of change of conversion over time, k is the reaction rate constant, and $f_{(\alpha)}$ is the reaction model.

Experimental determination is necessary to establish the relationship between the k and the conversion fraction, f(α). Weight loss data was used to calculate α over the range of 0–1, representing the progression of the reaction with respect to time or temperature. In thermal analysis, α at a specific time is mathematically expressed as follows (Eq. (21)):

$$\alpha = \frac{m_0 - m_t}{m_0 - m_f} \quad \text{(Eq. 21)}$$

where m_0 and m_f are the initial and final masses (mg), respectively, and m_t is the mass at a specific time. For a constant heating rate of $\beta = \frac{dT}{dt}$, Eq. (20) is expressed as follows (Eq. (22)):

$$\frac{d\alpha}{dT} = \beta^{-1} f_{(\alpha)} k_{(T)} \quad \text{(Eq. 22)}$$

After performing integration over the variables α and T, Eq. (21) becomes (Eq. (23)):

$$F_{(\alpha)} = \int_0^{\alpha} \frac{d\alpha}{f_{(\alpha)}} = \beta^{-1} \int_{T_0}^{T} k_{(T)} dT \quad \text{(Eq. 23)}$$

The Arrhenius equation is widely recognized as the most effective model for describing the temperature dependency of the rate $k_{(T)}$ (Eq. 24):

$$k_{(T)} = A exp\left(-\frac{E}{RT}\right) \quad \text{(Eq. 24)}$$

Here, A is the pre-exponential factor, E is the activation energy, and R is the gas constant. By combining Eqs. (23) and (24), the following expression is derived (Eq. (25)):

$$F_{(\alpha)} = A\beta^{-1} \int_{T_0}^{T} exp\left(-\frac{E}{RT}\right) dT \quad \text{(Eq. 25)}$$

When the initial temperature T_0 is much lower than the temperature at which the reaction rate becomes measurable, the lower limit of the temperature integral can be neglected. By introducing variable x as $-\frac{E}{RT}$, the following expression is derived (Eq. (26)):

$$F_{(\alpha)} = \left(\frac{AE}{\beta R}\right)\left\{ -\frac{e^x}{x} + \int_{-\infty}^{x} \left(\frac{e^x}{x}\right) dx \right\} = \left(\frac{AE}{\beta R}\right) \rho_{(x)} \quad \text{(Eq. 26)}$$

The expressions enclosed in curly brackets in Eq. (26) are represented as $\rho_{(x)}$ and include the exponential integral, which cannot be integrated analytically. Nevertheless, Doyle [44,45], was the first to observe that the logarithm of $\rho_{(x)}$ is approximately linear when plotted against x. Based on this observation, the following approximate relationship was proposed (Eq. (27)):

$$\ln \rho_{(x)} \cong -5.3305 + 1.052x \quad \text{(Eq. 27)}$$

By logarithmically transforming Eq. (26) and combining it with Eq. (27), the following expression is obtained (Eq. (28)):

$$ln\, F_{(\alpha)} \cong ln\frac{AE}{R} - ln\, \beta - 5.3305 + 1.052\frac{E}{RT} \quad \text{(Eq. 28)}$$

Hence, if a set of experiments is conducted at various heating rates, β_1, β_2, β_3, …, β_j, and $T_{k,j}$ represents the temperature at which a specific conversion fraction α_k is attained under heating rate β_j, plotting the logarithm (or natural logarithm) of β_j against $\frac{1}{T_{k,j}}$ for each conversion fraction α_1, α_2, α_3, …, α_k generates k isoconversion lines. The slopes of these lines determined using Eq. (28) yields (Eq. (29)):

$$\text{Slope} \cong 1.052\,\frac{E}{R}\left(\text{for ln } \beta_j \text{ vs } T_{k,j}^{-1}\right);\ (\alpha = \alpha_k) \quad \text{(Eq. 29)}$$

Therefore, E at α_k was determined by plotting $\ln\beta_j$ vs. $\frac{1}{T_{k,j}}$. The linearity of the slope, observed when considering three or more β values, was used to test the temperature invariance of E. Furthermore, any variation in E with respect to α_k can be identified by comparing the slopes at different α_k values.

In this study, isoconversion models were used to assess kinetic parameters. The TG curves were analyzed to determine E and A. Fig. 9 presents the TG curves of the AUC samples under non-isothermal conditions, including four distinct heating rates (10, 15, 20, and 30 °Cmin^{-1}). Analysis of these curves indicated that the temperature range of the decomposition reaction is dependent on the heating rate.

As the heating rate increases, the TG curves shift towards higher temperatures. Differences in the mass loss rates during heating at 10 and 30 °Cmin^{-1} are observed in the TG profiles. Furthermore, the maximum decomposition rate and the temperature at which it occurred increase with increasing heating rate, increasing from 217 °C at 10 °Cmin^{-1} to 240 °C at 30 °Cmin^{-1}. The influence of the heating rate on AUC decomposition is described by the mass loss data and temperature range corresponding to different heating rates (Table 6). Higher decomposition rates at higher heating rates were previously documented in studies of uranyl compounds [46].

The kinetic data for the thermal decomposition of AUC into UO_3 were obtained using the isoconversion method by determining the temperature at specific α values by conducting experiments at various β. A linear relationship was observed by plotting $\ln\beta$ against $\frac{1}{T}$ (Eq. (28)), as shown in Fig. 10. The E and A values were determined from the slopes of these linear correlations using Eq. (29). Table 7 presents the E values calculated using the isoconversion method for selected α values (0.1–0.8) corresponding to heating rates of 10, 15, 20, and 30 °Cmin^{-1}. The E determined by the isoconversion method varies within a narrow range and steadily increases from 82.41 kJmol^{-1} ($\alpha = 0.1$) to 92.69 kJmol^{-1} ($\alpha = 0.8$), with an average value of 85.80 ± 3.30 kJmol^{-1} and a coefficient of variation of 3.84%. The A values range from 3.68×10^{10} to 9.63×10^{10} s^{-1}, with an average value of $5.37 \pm 2.11 \times 10^{10}$ s^{-1}.

The E of AUC precipitation was determined to be in the range of 50–100 kJmol^{-1}, consistent with the values presented in previous studies [39–42,46]. Girgis and Rofail [39] conducted DTA–TG analyses on AUC in air and reported an average E of 83 kJmol^{-1}. Korichi et al. [40,41], utilized isoconversion methods to assess the kinetic parameters of the thermal decomposition of AUC in argon considering various α values (0.1–0.8) and calculated E values of 43.75–82.23 kJmol^{-1} and A values of 2.48×10^5–2.71×10^{10} s^{-1}. In a study conducted by Kim et al. [42], the thermal decomposition kinetics of AUC were examined using an isothermal TG reactor in an N_2 environment. The results revealed that, as the particle size increased, the reaction rate increased, whereas E decreased. Specifically, for an AUC powder fraction with a mean size of 42 μm, E was 68.9 kJmol^{-1}. Qingren and Shifang [46] investigated the thermal decomposition kinetics of AUC in N_2 using a non-isothermal approach, giving $E = 105.5$ kJmol^{-1} and $A = 2.17 \times 10^{10}$ s^{-1}. Hence, the E values obtained for the thermal decomposition of AUC into UO_3 are consistent with those reported in the literature.

3.3.3. *Conversion of UO_3 into U_3O_8*

In the dTG curve (Fig. 8), a plateau of constant weight was observed between 400 and 550 °C. The UO_3 begins to transform into U_3O_8 at 550 °C and continues over a wide temperature range (to well above 900 °C), resulting in a final weight loss of 2.3%.

During the transformation of UO_3 into U_3O_8, two peaks were observed in the dTG curve at temperatures of 618 and 678 °C (Fig. 8). This indicates that the conversion of UO_3 into U_3O_8 occurs via the formation of an intermediate compound before the final formation of U_3O_8. To determine this intermediate compound, we subjected the AUC sample to thermal decomposition at 800 °C, and the resulting sample was analyzed using XRD to identify the uranium-oxide components. Fig. 11 shows the XRD spectrum of the uranium oxide sample obtained after heating AUC at 800 °C for 6 h. Fig. 12 shows a photograph of U_3O_8 formed at 800 °C, which was covered with a yellow uranium oxide layer. The XRD spectrum (Fig. 11) shows that an intermediate compound of uranium oxide was formed. Several studies have reported similar evidence for the formation of intermediate compounds during the decomposition of UO_3 to U_3O_8. Previous studies [24,40,41], investigated the transformation of UO_3 into U_3O_8 in a nitrogen environment and found that the amorphous phase of UO_3 crystallizes into α-UO_3 before it decomposes into U_3O_8. The crystallization of amorphous UO_3 into α-UO_3 occurs in the temperature range of 400–480 °C, while the reduction of UO_3 into U_3O_8 occurs at 490–600 °C. The behavior observed in an argon environment is similar to that in nitrogen, where α-UO_3 is formed at 400–480 °C, and U_3O_8 starts to form at 490 °C and continues until 590 °C. The formation of U_3O_8 after AUC decomposition occurs over the temperature range of approximately 520–570 °C in an inert gas environment. Under oxygen, the formation of U_3O_8 occurs at approximately 550–630 °C.

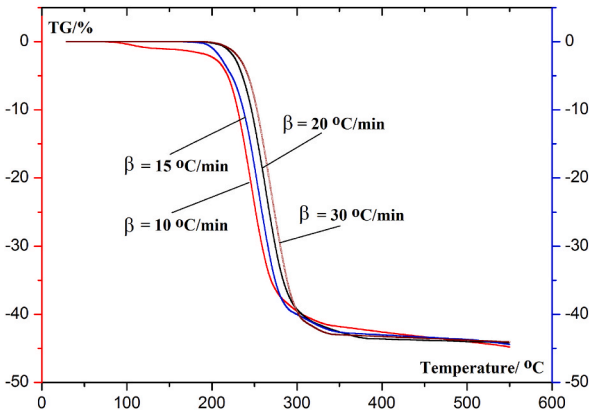

Fig. 9. TG of weight loss curves of AUC decomposition in air environment at four heating rates: 10 °Cmin^{-1}, 15 °Cmin^{-1}, 20 °Cmin^{-1} and 30 °Cmin^{-1}.

Table 6
The mass loss data and temperature range for the decomposition of AUC at different heating rates.

Heating rate β ($^oCmin^{-1}$)	T_i (^oC)	T_f (^oC)	T_{pick} (^oC)	Weight loss (%)
10	150	350	217	44.01
15	162	356	226	44.44
20	173	365	234	44.20
30	184	370	240	43.96

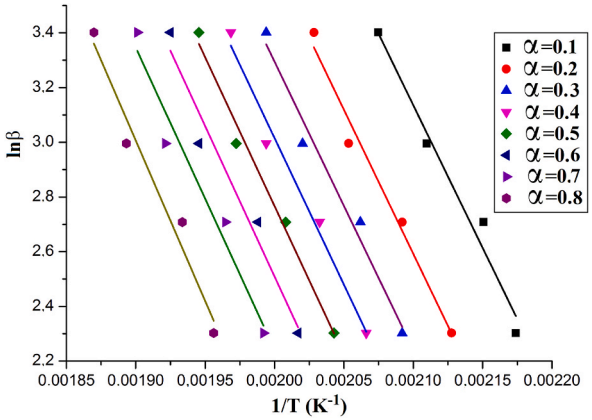

Fig. 10. The isoconvensional curves of AUC at different conversion fraction α.

Table 7
Kinetic parameters for the AUC decomposition to UO_3.

α	E ($kJmol^{-1}$)	A (s^{-1})	R^2
0.1	82.41	3.68×10^{10}	0.98
0.2	83.28	3.87×10^{10}	0.98
0.3	83.31	4.13×10^{10}	0.98
0.4	84.67	4.33×10^{10}	0.98
0.5	85.91	4.40×10^{10}	0.99
0.6	86.86	5.45×10^{10}	0.97
0.7	87.28	7.44×10^{10}	0.96
0.8	92.69	9.63×10^{10}	0.97
Average	85.80 ± 3.30	$5.37 \pm 2.11 \times 10^{10}$	
CV	3.84%	39.28%	

CV is coefficient of variation.

Thus, the transformation of ex-AUC UO_3 into U_3O_8 occurs in two stages: (i) conversion of UO_3 into an intermediate compound, e.g., the transformation of amorphous UO_3 into α-UO_3, which occurs at 550–650 °C; and (ii) conversion of α-UO_3 into $2UO_3{\cdot}UO_2$ at 650 to >800 °C.

3.4. Sintering of U_3O_8

The covalent bonding states of uranium in its oxides can vary because of the partially filled 5f shells. The predominant oxidation states are U^{4+} in UO_2 and U^{6+} in UO_3, which are the most stable forms. U^{5+} has also been observed in specific halocomplexes and hyperstoichiometric oxides such as U_2O_5 [47]. As another stable uranium oxide, U_3O_8 contains both U^{4+} and U^{6+}. Investigating the structures of higher uranium oxides in various extreme environments is crucial because these phases may form at different stages within nuclear reactors under high-temperature and high-pressure conditions.

In nuclear research reactor systems, the temperature inside the nuclear fuel rod, which contains U_3O_8 or UO_2 as the nuclear fuel, must withstand extremely high temperatures during operation; the highest temperature can reach 1800 °C. Therefore, studies on the sintering of U_3O_8 were conducted within the temperature range of 1000–1800 °C. The XRD spectrum of the U_3O_8 sample sintered at 1000 °C (Fig. 13) indicates that multiphase U_3O_8 was formed. However, the structures of U_3O_8 samples sintered at 1400 °C and 1800 °C were mostly single-phase (Fig. 14).

The XRD spectra (Figs. 13 and 14) show that the ex-AUC U_3O_8 powder is α-U_3O_8 with an orthorhombic structure with unit-cell parameters of a = 6.682 (1) Å, b = 11.866 (6) Å, and c = 4.296 (8) Å, angles of α = β = γ = 90°, and a space group of *C2mm*. Previous studies have confirmed the structure of α-U_3O_8 [47–50]. These studies revealed that the uranium atoms in α-U_3O_8 are

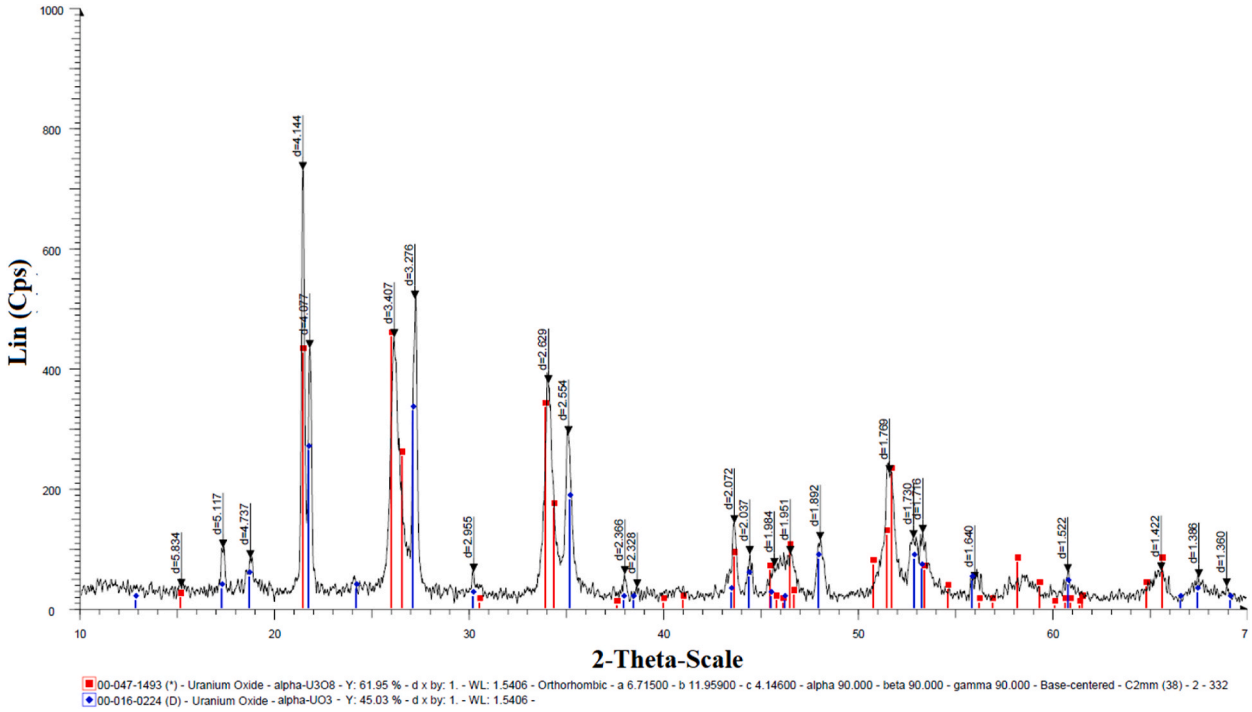

Fig. 11. The XRD spectrum of U_3O_8 at AUC conversion temperature of 800 °C.

Fig. 12. The photograph of uranium oxide at conversion temperature of 800 °C.

coordinated with oxygen in a 7-fold manner. Five oxygen atoms lie on the same plane, while the remaining two oxygen atoms are positioned on either side of the plane, forming a pentagon-based bipyramidal structure. The refined unit cell parameters of α-U_3O_8 were reported as follows: a = 6.751 (1) Å, b = 11.978 (2) Å, and c = 4.1607 (8) Å in the *C2mm* space group. Therefore, our studies on the structure of α-U_3O_8 are in good agreement with those presented in the existing literatures.

Fig. 15a and b depicted an SEM micrograph and the particle size distribution, respectively, of the ex-AUC U_3O_8 powder obtained at a sintering temperature of 1000 °C. The average particle size of the U_3O_8 is approximately 25 μm, which is similar to that of the original AUC powder. Fig. 16a and b showed SEM micrographs of the ex-AUC U_3O_8 nuclear material sintered at 1400 °C and 1800 °C, respectively. Interestingly, the particle size of U_3O_8 did not change significantly with increasing sintering temperature.

The research findings indicate no evidence of phase transformation occurring for the U_3O_8 powder sintered within the temperature range of 1000–1800 °C. However, the sample densities significantly increased with increasing sintering temperature, from approximately 7.0 gcm^{-3} at 1000 °C to 7.8 gcm^{-3} at 1400 °C. The density of the U_3O_8 nuclear material was determined according to the ASTM C373-88 standard. Thus, the ex-AUC U_3O_8 nuclear material has high thermal stability, which is crucial for a high-quality nuclear fuel

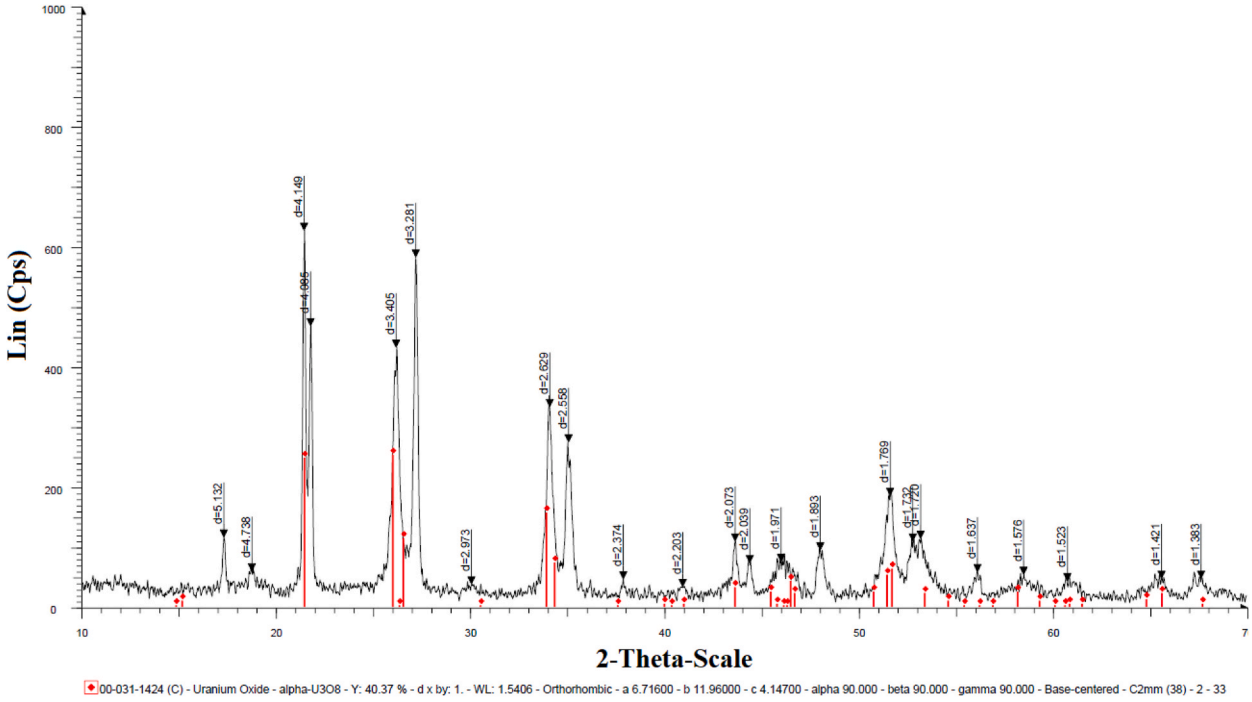

Fig. 13. The XRD spectrum of U_3O_8 at sintering temperature of 1000 °C.

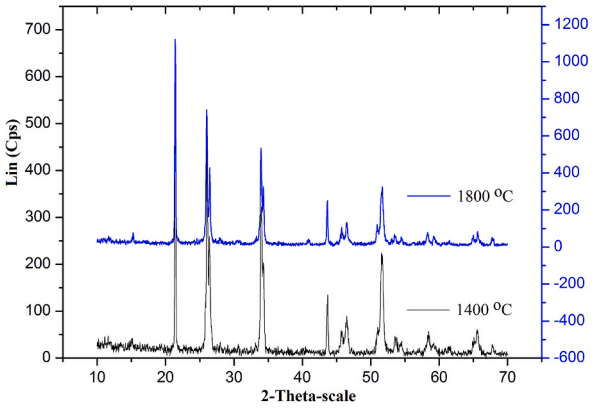

Fig. 14. The XRD spectrum of U_3O_8 at sintering temperature of 1400 °C and 1800 °C.

for use under research reactor conditions.

4. Conclusions

A comprehensive study was performed based on a series of AUC precipitation experiments, with particular focus on the formation of pure AUC crystals. Our findings indicate that at a C/U molar ratio below 6, AUF can form as an intermediate product, whereas C/U > 6 is required to form pure AUC crystals. The results of XRD and thermal analyses confirmed that the AUC crystal had a monoclinic structure (space group $C2/c$) with lattice constants $a = b = 10.06$ (1) Å, $c = 12.86$ (2) Å, $\alpha = \gamma = 90°$, and $\beta = 96.42°$, with a chemical formula of $(NH_4)_4UO_2(CO_3)_3$, which are in good agreement with the literature. The optimal parameters for AUC precipitation were a uranium concentration in the UO_2F_2 solution of 100 gL^{-1}, $(NH_4)_2CO_3$ precipitant concentration of 400 gL^{-1}, and C/U ratio of 8. Under these conditions, the AUC precipitation efficiency exceeds 95%, with large particle sizes (~24 μm) and a lower impurity content than that specified in the ASTM C776-06 standard. Kinetic studies of AUC precipitation revealed that the reaction followed second-order kinetics with a rate constant of 0.258 $Lmol^{-1}min^{-1}$ at 298.15 K (25 °C).

During AUC decomposition into U_3O_8 under air, UO_3 formed as an intermediate compound at 150–370 °C. The kinetic constant for the thermal decomposition of AUC into UO_3 was 85.80 ± 3.30 $kJmol^{-1}$, with a variation coefficient of 3.84% and pre-exponential

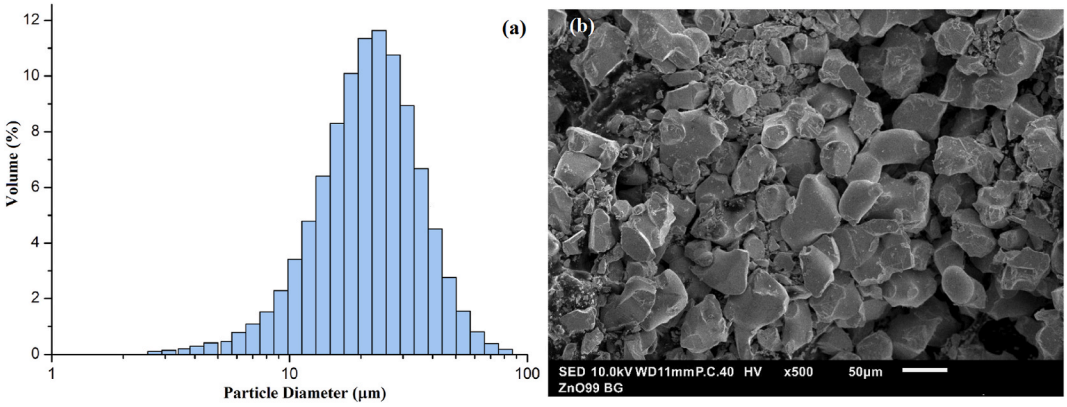

Fig. 15. The particle size distribution **(a)** and SEM microphotograph **(b)** of the ex-AUC U_3O_8 nuclear material at sintering temperature of 1000 °C.

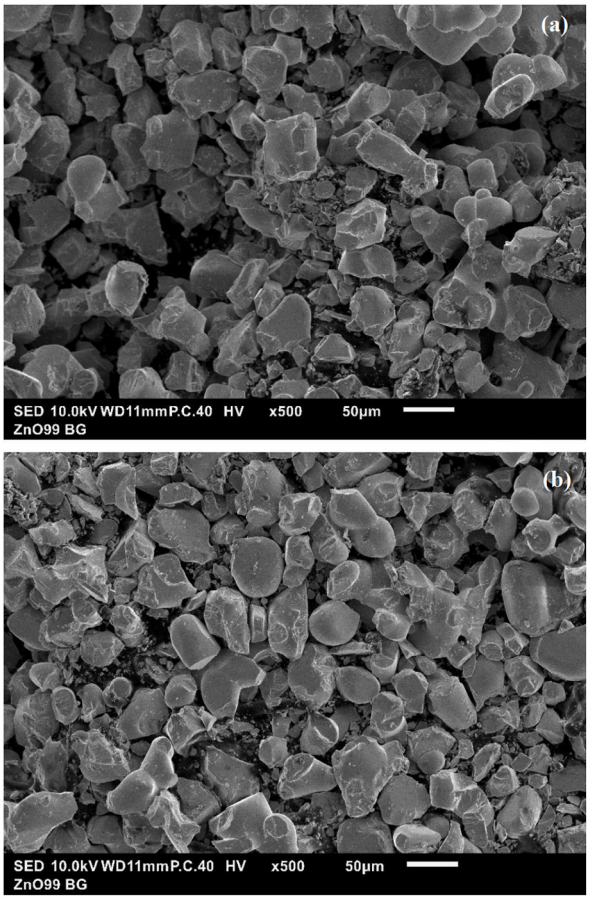

Fig. 16. The SEM microphotograph of the ex-AUC U_3O_8 materials at conversion temperature of 1400 °C **(a)** and 1800 °C **(b)**.

factor of $5.37 \pm 2.11 \times 10^{10}$ s^{-1} determined using the isoconversion method. This kinetic constant is consistent with those reported in the literature. The conversion of UO_3 into U_3O_8 takes place at temperatures from 550 °C to above 800 °C, and seems to involve the transformation of the amorphous UO_3 into α-UO_3, followed by $2UO_3{\cdot}UO_2$. Sintering of the U_3O_8 nuclear material was performed over a temperature range of 1000–1800 °C and XRD analysis confirmed mostly single-phase α-U_3O_8 with an orthorhombic structure. The unit cell parameters of α-U_3O_8 are a = 6.682 (1) Å, b = 11.866 (6) Å, c = 4.296 (8) Å, and $\alpha = \beta = \gamma = 90°$ with a space group of *C2mm*, which agrees well with existing literature. The crystal structure and particle size of the ex-AUC U_3O_8 nuclear material remained almost unchanged at different sintering temperatures. However, the density of the U_3O_8 nuclear material increases with increasing sintering

temperature, reaching approximately 7.8 gcm^{-3} at 1400 °C.

Our experiments on the precipitation of AUC from a UO_2F_2 solution and its subsequent conversion into U_3O_8 were aimed at producing high-density U_3O_8 nuclear material for the low-enriched uranium (LEU) nuclear fuel used in research reactors.

Data availability statement

Data will be made available on request.

CRediT authorship contribution statement

Nguyen Trong Hung: Writing – review & editing, Writing – original draft, Visualization, Validation, Supervision, Software, Resources, Project administration, Methodology, Investigation, Funding acquisition, Formal analysis, Data curation, Conceptualization. **Le Ba Thuan:** Writing – review & editing, Formal analysis, Data curation, Conceptualization. **Nguyen Thanh Thuy:** Writing – review & editing, Investigation, Formal analysis, Data curation, Conceptualization. **Hoang Sy Than:** Writing – review & editing, Formal analysis, Data curation, Conceptualization. **Dinh Van Phuc:** Writing – review & editing, Formal analysis, Data curation, Conceptualization. **Jin-Young Lee:** Writing – review & editing, Resources, Funding acquisition, Formal analysis, Data curation, Conceptualization. **Rajesh Kumar Jyothi:** Writing – review & editing, Formal analysis, Data curation, Conceptualization.

Declaration of competing interest

The authors declare the following financial interests/personal relationships which may be considered as potential competing interests:Jin-Young Lee reports financial support was provided by Korea Institute of Geoscience and Mineral Resources (KIGAM). Rajesh Kumar Jyothi reports a relationship with CSIRO Mineral Resources (CMR) that includes: employment. If there are other authors, they declare that they have no known competing financial interests or personal relationships that could have appeared to influence the work reported in this paper.

Acknowledgments

Dr. Nguyen Trong Hung expresses his sincere gratitude to the authorities of VINATOM and the MOST for funding this research work through the Ministry project No. DTCB.10/22/VCNXH: “Study on preparation of the high density compound U_3O_8 orienting to LEU nuclear fuel for research reactor”. The Korean researchers express their gratitude for a National Research Council of Science & Technology (NST) grant from the Korean government (MSIT) (No. CRC-15-06-KIGAM).

References

[1] IAEA, Nuclear Fuel Cycle Information System, 2009. IAEA-TECDOC-1613.
[2] Xuezhi Wu, Bangyue Yin, Mechanism and properties of UO_2–Graphene composite fuel prepared by in situ synthesis, Crystals 12 (2022) 230, https://doi.org/10.3390/cryst12020230.
[3] Moch Setyadji, Fitrotun Aliyah, Characteristics of uranium dioxide (UO_2) kernel produced by sintering process using modified sintering reactor, IOP Conf. Series: Materials Science and Engineering 553 (2019) 012040, https://doi.org/10.1088/1757-899X/553/1/012040.
[4] J.B. Silva Neto, E.F. Urano de Carvalho, R.H.L. Garcia, A.M. Saliba-Silva, H.G. Riella, M. Durazzo, Production of UF_4 from the effluent generated in the reconversion via ammonium uranyl carbonate, Nucl. Eng. Technol. 49 (8) (2017) 1711–1716, https://doi.org/10.1016/j.net.2017.07.019.
[5] Y.W. Lee, M.S. Yang, Characterization of HWR fuel pellets fabricated using UO2 powders from different conversion processes, J. Nucl. Mater. 178 (2–3) (1991) 217–226, https://doi.org/10.1016/0022-3115(91)90389-O.
[6] https://world-nuclear.org/information-library/research-reactors.aspx.
[7] Balakrishna Palanki, Some factors affecting densification and grain growth in the sintering of uranium dioxide-a brief review, J. Nucl. Mater. 550 (2021) 152918, https://doi.org/10.1016/j.jnucmat.2021.152918.
[8] E.K. Papynov, O.O. Shichalin, A.Yu Mironenko, A.V. Ryakov, I.V. Manakov, P.V. Makhrov, I.Yu Buravlev, I.G. Tananaev, V.A. Avramenko, V.I. Sergienko, Synthesis of high-density pellets of uranium dioxide by spark plasma sintering in dies of different types, Radiochemistry 60 (4) (2018) 362–370, https://doi.org/10.1134/S1066362218040045. Published in Radiokhimiya, 2018, Vol. 60, No. 4, pp. 311–318.
[9] N.P. Galkin, U.D. Veryatin, I.F. Yakhonin, A.F. Lugonov, Yu M. Dymkov, The conversion of uranium hexafluoride to dioxide, Translated from Atomnaya Energiya 52 (1) (1982) 36–39, https://doi.org/10.1007/BF01121773. Original article submitted May 20, 1980.
[10] Sven G. Brandberg, The conversion of uranium hexafluoride to uranium dioxide, Nucl. Technol. 18 (2) (1973) 177–184, https://doi.org/10.13182/NT73-A31286.
[11] Tyler L. Spano, Antonio Simonetti, Loretta Corcoran, Philip A. Smith, Stefanie R. Lewis, Peter C. Burns, Comparative chemical and structural analyses of two uranium dioxide fuel pellets, J. Nucl. Mater. 518 (2019) 149–161, https://doi.org/10.1016/j.jnucmat.2019.02.038.
[12] Erik C. Abbott, Alexandria Brenkmann, Craig Galbraith, Joshua Ong, Ian J. Schwerdt, Brent D. Albrecht, Tolga Tasdizen, W. Luther, I.V. McDonald, Dependence of UO_2 surface morphology on processing history within a single synthetic route, Radiochim. Acta (2019), https://doi.org/10.1515/ract-2018-3065.
[13] H. Tel, M. Eral, Investigation of production conditions and powder properties of AUC, J. Nucl. Mater. 231 (1996) 165, https://doi.org/10.1016/0022-3115(96)00354-6.
[14] A. Marajofsky, L. Perez, J. Celora, On the dependence of characteristics of powders on the AUC process parameters, J. Nucl. Mater. 178 (1991) 143–151, https://doi.org/10.1016/0022-3115(91)90379-L.
[15] W. Timmermans, A. Van Heck-Hennen, F. Gorle, R. de Batist, Sintering characterization of UO2 powders, J. Nucl. Mater. 71 (2) (1978) 256–267, https://doi.org/10.1016/0022-3115(78)90423-3.
[16] C.S. Choi, J.H. Park, E.H. Kim, H.S. Shin, I.S. Chang, The influence of AUC powder characteristics on UO_2 pellets, J. Nucl. Mater. 153 (1988) 148, https://doi.org/10.1016/0022-3115(88)90206-1.
[17] Z.X. Song, X.W. Huang, Defluorination behavior and mechanism of uranium dioxide, J. Radioanal. Nucl. Chem. 237 (1–2) (1977) 81–84, https://doi.org/10.1007/BF02386666.

[18] N. Lindman, The kinetics of the elimination of fluorine from uranylfluoride/uraniumdioxide pellets, J. Nucl. Mater. 66 (1–2) (1977) 23–36, https://doi.org/10.1016/0022-3115(77)90130-1.

[19] S. Chegrouche, A. Kebir, Study of ammonium uranyl carbonate re-extraction-crystallization process by ammonium carbonate, Hydrometallurgy 28 (2) (1992) 135–147, https://doi.org/10.1016/0304-386X(92)90126-K.

[20] Maw-Chwain Lee, Chung-Jyi Wu, Conversion of UF6 to UO2: a quasi-optimization of the ammonium uranyl carbonate process, J. Nucl. Mater. 185 (2) (1991) 190–201, https://doi.org/10.1016/0022-3115(91)90335-5.

[21] Yi-Ming Pan, Che-Bao Ma, Nien-Nan Hsu, The conversion of UO2 via ammonium uranyl carbonate: study of precipitation, chemical variation and powder properties, J. Nucl. Mater. 99 (2–3) (1981) 135–147, https://doi.org/10.1016/0022-3115(81)90182-3.

[22] Kan-Sen Chou, Ding-Yi Lin, Mu-Chang Shieh, Precipitation studies of ammonium uranyl carbonate from UO2F2 solutions, J. Nucl. Mater. 165 (2) (1989) 171–178, https://doi.org/10.1016/0022-3115(89)90246-8.

[23] M.H. Sadeghi, M. Outokesh, M. Habibi Zare, Production of high quality ammonium uranyl carbonate from "uranyl nitrate + carbonate" precursor solution, Prog. Nucl. Energy 122 (2020) 103270, https://doi.org/10.1016/j.pnucene.2020.103270.

[24] P. Govindan, A. Palamalai, K.S. Vijayan, S. Subbuthai, S. Murugesan, S.V. Mohan, R.V. Subba Rao, Development of a reconversion method for uranyl nitrate to oxide in the reconversion step of reprocessing of irradiated fuel, J. Radioanal. Nucl. Chem. 254 (1) (2002) 65–70, https://doi.org/10.1023/A:1020837430070.

[25] P. Govindan, A. Palamalai, T. Vasudevan, K.S. Vijayan, R.V. Subba Rao, M. Venkataraman, R. Natarajan, Ammonium uranyl carbonate (AUC) based process of simultaneous partitioning and reconversion for uranium and plutonium in fast breeder reactors (FBRs) fuel reprocessing, J. Radioanal. Nucl. Chem. 295 (1) (2012), https://doi.org/10.1007/s10967-012-1831-x.

[26] V. Baran, F. Skvor, V. Vosecek, Formation of the ammonium-uranyl-carbonate complexes of the type $(NH_4[UO_2(CO_3)_3]$ prepared by precipitative reextraction, Inorg. Chim. Acta. 81 (1984) 83–89, https://doi.org/10.1016/S0020-1693(00)88739-3.

[27] Hung Nguyen Trong, Le Ba Thuan, Tran Chi Thanh, Nhuan Hoang, Do Van Khoai, Nguyen Van Tung, Jin Young Lee, Rajesh Kumar Jyothi, Modeling the UO_2 ex-AUC pellet process and predicting the fuel rod temperature distribution under steady-state operating condition, J. Nucl. Mater. 504 (2018) 191–197, https://doi.org/10.1016/j.jnucmat.2018.03.027.

[28] Hung Nguyen Trong, Le Ba Thuan, Nguyen Van Tung, Nguyen Thanh Thuy, Jin Young Lee, Rajesh Kumar Jyothi, The UO_2 ex-ADU powder preparation and pellet sintering for optimum efficiency: experimental and modeling studies, J. Nucl. Mater. 496 (2017) 177–181, https://doi.org/10.1016/j.jnucmat.2017.09.026.

[29] Hung Nguyen Trong, Le Ba Thuan, Do Van Khoai, Jin Young Lee, Rajesh Kumar Jyothi, Modeling conversion of ammonium diuranate (ADU) into uranium dioxide (UO_2) powder, J. Nucl. Mater. 479 (2016) 483–488, https://doi.org/10.1016/j.jnucmat.2016.07.045.

[30] Hung Nguyen Trong, Le Ba Thuan, Do Van Khoai, Jin Young Lee, Rajesh Kumar Jyothi, Brandon mathematical model describing the effect of calcination and reduction parameters on specific surface area of UO_2 powders, J. Nucl. Mater. 474 (2016) 150–154, https://doi.org/10.1016/j.jnucmat.2016.03.021.

[31] Eung Ho Kim, Cheong Song Choi, Jin Ho Park, Seon Gil Kwon, In Soon Chang, A study on morphology and chemical composition of precipitates produced from UO2(NO3)2-(NH4)2CO3 solution, J. Nucl. Mater. 209 (3) (1994) 301–305, https://doi.org/10.1016/0022-3115(94)90267-4.

[32] A. Boualia, A. Mellah, Précipitation de l'AUC par NH3 et CO2 à partir des solutions de nitrate d'uranyle. Precipitation of AUC by NH3 and CO2 from an uranyl nitrate solution, Hydrometallurgy 21 (3) (1989) 331–344, https://doi.org/10.1016/0304-386X(89)90006-6.

[33] Oleg Pokrovskiy, Anton Vorobei, Yaroslav Zuev, Mikhail Kostenko, Valery Lunin, Investigation of precipitation selectivity and particle size concentration dependences in supercritical antisolvent method via online supercritical fluid chromatography, Adv. Powder Technol. 31 (6) (2020) 2257–2266, https://doi.org/10.1016/j.apt.2020.03.022.

[34] N.H. Rofail, Infrared and X-ray diffraction spectra of ammonium uranyl Carbonate, Mater. Chem. Phys. 36 (1994) 241–245, https://doi.org/10.1016/0254-0584(94)90036-1.

[35] R. Graziani, G. Bombieri, E. Forsellini, Crystal structure of tetra-mmonium uranyl tricarbonate, J. Chem. Soc., Dalton Trans. 19 (1972) 2059–2061, https://doi.org/10.1039/DT9720002059.

[36] Tae-Joon Kim, Kyung-Chai Jeong, Jin-Ho Park, In-Soon Chang, Cheong-Song Choi, Crystallization characteristics of ammonium uranyl carbonate (AUC) in ammonium carbonate solutions, J. Nucl. Mater. 209 (1994) 306–314, https://doi.org/10.1016/0022-3115(94)90268-2.

[37] L. Hälldahl, M. Nygren, Thermal analysis studies of the reactions occurring during the decomposition of ammonium uranyl carbonate in different atmospheres, J. Nucl. Mater. 138 (1986) 99–106, https://doi.org/10.1016/0022-3115(86)90260-6.

[38] L. Hälldahl, M. Nygren, TG, DSC, X-ray and electron diffraction studies of intermediate phases in the reduction of ammonium uranyl carbonate to UO_2, Thermochim. Acta 72 (1–2) (1984) 213–218, https://doi.org/10.1016/0040-6031(84)85076-5.

[39] B.S. Girgis, N.H. Rofail, Decomposition-reduction stages of ammonium uranyl carbonates under different atmospheres, Thermochim. Acta 196 (1–3) (1992) 105–115, https://doi.org/10.1016/0040-6031(92)85010-S.

[40] S. Korichi, F. Mernache, F. Benaouicha, N. Aoudia, A. Amrane, S. Hadji, Thermal behavior and kinetic modeling of $(NH_4)_4UO_2(CO_3)_3$ decomposition under non-isothermal conditions, J. Radioanal. Nucl. Chem. 314 (2017) 923–934, https://doi.org/10.1007/s10967-017-5444-2.

[41] Korichi Smain, Aoudia Nacera, Benelmaddjat Hanane, Kaci Smina, Ousmaal Nafissa, Kinetic studies of isothermal decomposition of $(NH_4)_4UO_2(CO_3)_3$ to uranium oxide, Prog. React. Kinet. Mech. 45 (2019) 1–12, https://doi.org/10.1177/1468678319888629.

[42] E.H. Kim, J.J. Park, J.H. Park, I.S. Chang, C.S. Choi, S.D. Kim, Thermal decomposition kinetics of ammonium uranyl carbonate, J. Nucl. Mater. 209 (3) (1994) 294–300, https://doi.org/10.1016/0022-3115(94)90266-6.

[43] A. Mellah, S. Chegrouche, M. Barkat, The precipitation of ammonium uranyl carbonate (AUC): thermodynamic and kinetic investigations, Hydrometallurgy 85 (2007) 163–171, https://doi.org/10.1016/j.hydromet.2006.08.011.

[44] J.H. Flynn, The isoconversional method for determination of energy of activation at constant heating rates, J. Therm. Anal. 27 (1983) 95–102, https://doi.org/10.1007/BF01907325.

[45] C.D. Doyl, Estimating isothermal life from thermogravimetric data, J. Appl. Polym. Sci. 6 (24) (1962) 639–642, https://doi.org/10.1002/app.1962.070062406.

[46] Qingren Ge, Shifang Kang, Study of AUC thermal decomposition kinetics in nitrogen by a non-isothermal method, Thermochim. Acta 116 (1987) 71–77, https://doi.org/10.1016/0040-6031(87)88166-2.

[47] R.E. Rundle, N.C. Baenziger, A.S. Wilson, R.A. McDonald, The structures of the carbides, nitrides and oxides of uranium, J. Am. Chem. Soc. 70 (1948) 99–105, https://doi.org/10.1021/ja01181a029.

[48] R. Herak, B. Jovanovic, On the existence of δ-U_3O_8, Inorg. Nucl. Chem. Lett. 5 (1969) 693–697, https://doi.org/10.1016/0020-1650(69)80168-6.

[49] B.O. loopstra, Neutron diffraction investigation of U_3O_8, Acta Crystallogr. 17 (1964) 651–654, https://doi.org/10.1107/S0365110X6400158X.

[50] F.X. Zhang, M. Lang, J.W. Wang, W.X. Li, K. Sun, V. Prakapenka, R.C. Ewing, High-pressure U_3O_8 with the fluorite-type structure, J. Solid State Chem. 213 (2014) 110–115, https://doi.org/10.1016/j.jssc.2014.02.012.